academicJournals

Vol. 8(31), pp. 1495-1511, 18 August, 2013
DOI 10.5897/SRE11.2183
ISSN 1992-2248 © 2013 Academic Journals
http://www.academicjournals.org/SRE

Scientific Research and Essays

Full Length Research Paper

Stability analysis for a turbocharger rotor system under nonlinear hydrodynamic forces

Hao Zhang[1,2], Zhanqun Shi[1,3]*, Shunxin Zhang[1], Fengshou Gu[2] and Andrew Ball[2]

[1]Hebei University of Technology, Tianjin, 300130, China.
[2]Huddersfield University, Huddersfield, HD1 3DH, UK.
[3]State Key Laboratory of Mechanical Science and Vibration, Shanghai Jiaotong University, Shanghai, 200240, China.

Accepted 2 October, 2012

Turbocharger is a high speed rotor system supported by a pair of floating ring bearings which comprise of double oil films. The stability of its rotor system is governed by not only the structure of the rotor but also by the nonlinear hydrodynamic force of two oil films. In this paper, a lumped dynamics model is developed for a turbocharger rotor system. In order to investigate the nonlinear behavior of the rotor system, the analytical expression of nonlinear hydrodynamic force of outer and inner oil films is derived on the basis of Capone oil film force model. Shooting method and continuation algorithm are used to obtain the periodic solution of the dynamics equation. Based on the numerical simulation results, the effects of rotor imbalance and lubricant feed pressure on the stability discipline and bifurcation behaviors are studied.

Key words: Turbocharger rotor system, nonlinear hydrodynamic force, stability analysis, bifurcation behaviors.

INTRODUCTION

Turbocharger has been widely used in vehicles to recycle the exhaust energy and boost engine power. The working speed of the turbocharger can reach 140,000 r/min and over. At such a high speed, even a weak vibration can lead to the failure of its rotor system. In order to ensure the turbocharger operating safely under the extreme working condition, it is meaningful to carry out the research on the vibration and the stability of the turbocharger rotor system.

The stability of a rotor bearing system is generally governed by hydrodynamic forces. Hagg (1956), Sternlicht (1959), Lund (1964, 1968) and Glienicke (1966) proposed a theory to describe dynamic characteristics of the journal bearing by using linearized coefficients such as stiffness and damping coefficients. In this theory, the hydrodynamic force is expressed by a function of displacement and velocity in the static equilibrium position. Reynolds Equation is solved to obtain the oil film pressure, which is then used to calculate the hydrodynamic force. However, the condition of the weak perturbation is sometimes not satisfied, thus the linearized result might be insufficient to describe the nonlinear behaviors of the rotor system. In order to reveal the mechanism of oil film instability, recently researchers have studied in depth the principle of the shaft motion based on the research of the nonlinear rotor system differential motion equation (Yang et al., 2004). Goldman and Muszynska (1994) studied the chaotic behavior of rotor/stator systems with rub-impacts. The analytical and numerical simulations show that the regular periodic vibration of the order of the synchronous, the subsynchronous and the chaos vibration are all accompanied by higher harmonics. Chu and Zhang (1998) investigated the nonlinear vibration characteristics

*Corresponding author. Email: z_shi@hebut.edu.cn. Tel: 0086 22 26582598.

of a rub-impact Jeffcott rotor. They found that when the rotational speed is increased, the grazing bifurcation, the quasi-periodic motion and chaotic motion occur after the rub-impact. Chang-Jian and Chen (2006a, 2006b, 2007a, 2007b) presented a series of papers on the nonlinear dynamics of rotor-bearing systems under nonlinear suspension and combined these with rub-impact effect, turbulent effect and micropolar lubricant. They found that many non-periodic responses occurred in the rotor-bearing systems. Fu et al. (2003) investigated the chaotic motions of a rotor system with a transverse crack by theoretical and numerical approaches.

The turbocharger is a flexible rotor system supported by a pair of floating ring bearings. The inner and outer oil films affect the rotor motion simultaneously that makes the stability discipline more complicated to be studied. Tatara (1970) stated that as soon as whirl appears in the inner film, the ring begins to spin and the bearing could stabilize the rotor system. Tanaka and Hori (1972) developed a dynamics model for a flexible rotor supported by floating ring bearings based on the infinitely short bearing theory and then the stable speed is estimated under different bearing parameters. By the comparison of predicted and experimental results acquired by Hill (1950) and Dworski (1964), it was demonstrated that the frequency of the oil film whirl was approximately one half of the sum of the shaft speed and the ring speed under medium pressure. Rohde and Ezzat (1980) reported that floating ring bearings have the potential to reduce the power loss of the automotive engine. Tatara (1970) carried out a linear stability analysis of the floating ring rotor bearing system. It was found that the unstable speed is sensitive to the outer bearing clearance and the thinner of the outer bearings clearance is, the wider speed range covered. Trippett and Dennis (1983) concluded that oil film whirl and whip is caused by shear effects between the inner and outer fluid films and will eventually reach a stable limit cycle. Howard (1999) discussed the possibility of replacing oil film bearings by air bearings in a diesel truck turbocharger. Aretakis et al. (2004) discussed the possibility of detecting the instability in the turbocharger rotor system by vibration and noise signals of the compressor impeller. By the signal features extraction, a bi-parametric criterion was established for determination of whether the compressor of the turbocharger operates in the stable stage. Chen et al. (1996) developed a model for a turbocharger turbine under pulsating inlet conditions. The one-dimensional unsteady flow method was applied to study the behavior of the turbine under steady and unsteady flow conditions. This model showed an improved prediction in the off-design condition. Kreuz-Ihli et al. (2000) utilized a commercial Navier-stokes solver to study the vibration of radial inflow turbines under the unsteady flow and then validated the model by experimental data collected from a Laser-Doppler velocimeter. Peat et al. (2006) presented a model for the passive acoustic behavior of a turbine impeller of an automotive turbocharger. Based on the knowledge of the rotor vibration, the effects of the primary noises, such as the gas pulsation and the exhaust tailpipe orifice, on the behavior of the turbine were studied. Payri et al., (1996, 2000) published a series of papers focusing on the investigation of the transient performance of turbocharged diesel engines and developed an action model for calculating the transient operation.

So far, most of the stability research is carried out based on the simplified model, such as Jeffcott rotor. However, the stability of the turbocharger rotor system, which is a high speed flexible rotor system supported by floating ring bearings, is still not clear. Therefore, in this paper, a lumped model is developed for the turbocharger rotor system. The analytical expression of the nonlinear hydrodynamic force is derived based on the Capone oil film force model. Following model development, the bending vibration of a turbocharger rotor system is calculated in MATLAB. Based on the simulation results, the effects of rotor imbalance and lubricant feed pressure on the stability of the turbocharger rotor system are investigated using the floquet theory and bifurcation analysis.

THEORY BACKGROUND

Dynamics equation of a rotor-bearing system

The dynamics equation of a rotor-bearing system with multi-degree of freedom is expressed by Equation (1), which can be transformed into a first order differential Equation (2) by the state-space method.

$$[\mathrm{M}]\{\ddot{\mathrm{U}}\}+[\mathrm{C}]\{\dot{\mathrm{U}}\}+[\mathrm{K}]\{\mathrm{U}\}=\{\mathrm{F}\} \quad (1)$$

$$\frac{\partial \mathrm{U}}{\partial \mathrm{t}}=\mathrm{F}(\mathrm{t}, \mathrm{U}, \Omega) \quad (2)$$

If the force vector on the right hand side of the Equation (2) does not depend on the time t, that is, $\mathrm{F}(\mathrm{t}, \mathrm{U}, \Omega)=\mathrm{F}(\mathrm{U}, \Omega)$, the system is called an autonomous system in mathematics; if the force vector is a function of a period T, that is, $\mathrm{F}(\mathrm{t}, \mathrm{U}, \Omega)=\mathrm{F}(\mathrm{t}+\mathrm{T}, \mathrm{U}, \Omega)$, the system is called a non-autonomous system. Due to the existence of the residual rotor imbalance, most of rotor-bearing systems belong to the non-autonomous system.

The periodic solution of the nonlinear dynamics equation

Numerical approach is a common approach in the

solution of the periodic solution of the nonlinear dynamics equation as the analytical solution is generally difficult to be obtained. Numerical integration method and shooting method, as two classical methods of the numerical approach, are widely used in solving the periodic solution. Numerical integration method is simple to apply but the obvious disadvantage of this method is that only the stable periodic solution can be solved. Compared to the numerical integration method, the shooting method, which transforms an initial value problem of a differential equation into a boundary value problem, shows more efficiently in the solution of the periodic solution. By combining the shooting method with the continuation method, both the stable and unstable periodic solution can be obtained simultaneously (Granas et al., 2012). The solution approach is detailed as follows:

According to the definition, the periodic solution of the nonlinear dynamics Equation (2) should meet the condition (3).

$$\mathrm{U}(\mathrm{t}) = \mathrm{U}(\mathrm{t}+\mathrm{T}) \tag{3}$$

By Poincaré map, the solution of the continuous dynamics system can be transformed into the solution of the fixed point. A Poincaré map with n+1 dimension is defined by Equation (4).

$$\sum = \{(\mathrm{U}, \mathrm{t}) \mid \mathrm{mod}(\mathrm{t}, \mathrm{T}) = 0\} \tag{4}$$

The fixed point u^* in the map should meet the periodic boundary condition (5).

$$\mathrm{G}(\mathrm{u}) = \mathrm{u} - \mathrm{P}(\mathrm{u}) \tag{5}$$

Equation (5) can be solved by Newton-Raphson iteration method, which is shown in Equation (6).

$$\mathrm{u}_{\mathrm{k}+1} = \mathrm{u}_{\mathrm{k}} - \left[\mathrm{G}_{\mathrm{u}}^{'}(\mathrm{u}_{\mathrm{k}})\right]^{-1}\mathrm{G}(\mathrm{u}_{\mathrm{k}}) \tag{6}$$

Differentiate Equation (6) with respect to u, we can obtain (7)

$$\mathrm{G}_{\mathrm{u}}^{'} = \mathrm{I} - \mathrm{P}_{\mathrm{u}}^{'} \tag{7}$$

Substitute (7) into (6), we can obtain (8)

$$\mathrm{u}_{\mathrm{k}+1} = \mathrm{u}_{\mathrm{k}} - \left[\mathrm{I} - \mathrm{P}_{\mathrm{u}}^{'}(\mathrm{u}_{\mathrm{k}})\right]^{-1}\left[\mathrm{u}_{\mathrm{k}} - \mathrm{P}(\mathrm{u}_{\mathrm{k}})\right] \tag{8}$$

The Jacobi matrix of Poincaré mapping, $\mathrm{P}_{\mathrm{u}}^{'}(\mathrm{u}_{\mathrm{k}})$ in Equation (8), is the solution of Equation (9) at t = T.

$$\begin{aligned}
&\frac{\partial \mathrm{U}}{\partial \mathrm{t}} = \mathrm{F}(\mathrm{t}, \mathrm{U}, \Omega)\\
&\mathrm{U}(0) = \mathrm{u}_{\mathrm{k}}\\
&\frac{\partial}{\partial \mathrm{t}}\left(\frac{\partial \mathrm{U}}{\partial \mathrm{U}_{\mathrm{o}}}\right) = \mathrm{F}_{\mathrm{u}}^{'}(\mathrm{t}, \mathrm{U}, \Omega)\left(\frac{\partial \mathrm{U}}{\partial \mathrm{U}_{\mathrm{o}}}\right)\\
&\frac{\partial \mathrm{U}}{\partial \mathrm{U}_{\mathrm{o}}}(0) = \mathrm{I}
\end{aligned} \tag{9}$$

The continuation algorithm is used to estimate initial values of the numerical integration. Initial values of the numerical integration under current parameters can be estimated by the periodic solution under previous parameters. The approach to estimate initial values under different rotational speeds of a rotor-bearing system is detailed as follows.

Differentiate Equation (2) with respect to U, Ω, we can obtain Equation (10).

$$\partial \mathrm{F}(\mathrm{U}, \Omega) = \mathrm{F}_{\mathrm{u}}^{'}(\mathrm{U}, \Omega)\partial \mathrm{U} + \mathrm{F}_{\Omega}^{'}(\mathrm{U}, \Omega)\partial \Omega \tag{10}$$

According to the principle of the homotopy continuation method, the relationship between the periodic solution under the current speed and initial iteration values under the next speed is expressed by Equation (11).

$$\begin{aligned}
&\mathrm{U}_{\mathrm{i}+1} = \mathrm{U}_{\mathrm{i}} - \left[\mathrm{I} - \mathrm{P}_{\mathrm{u}}^{'}(\Omega_{\mathrm{i}}, \mathrm{U}_{\mathrm{i}})\right]^{-1}\left[-\mathrm{P}_{\Omega}^{'}(\Omega_{\mathrm{i}}, \mathrm{U}_{\mathrm{i}})\right]\Delta\Omega\\
&\Omega_{\mathrm{i}+1} = \Omega_{\mathrm{i}} + \Delta\Omega
\end{aligned} \tag{11}$$

$\mathrm{P}_{\Omega}^{'}(\Omega_{\mathrm{i}}, \mathrm{U}_{\mathrm{i}})$ in Equation (11) is the solution of Equation (12) at t = T.

$$\begin{aligned}
&\frac{\partial \mathrm{U}}{\partial \mathrm{t}} = \mathrm{F}(\mathrm{t}, \Omega_{\mathrm{i}}, \mathrm{U})\\
&\mathrm{U}(0) = \mathrm{U}_{\mathrm{i}}\\
&\frac{\partial}{\partial \mathrm{t}}\left(\frac{\partial \mathrm{U}}{\partial \Omega}\right) = \mathrm{F}_{\Omega}^{'}(\mathrm{t}, \Omega_{\mathrm{i}}, \mathrm{U})\left(\frac{\partial \mathrm{U}}{\partial \Omega}\right)\\
&\frac{\partial \mathrm{U}}{\partial \Omega}(0) = 0
\end{aligned} \tag{12}$$

The stability of a rotor-bearing system

Due to the existence of the residual rotor imbalance, the rotor generally performs a synchronous motion at relatively low speeds, which maps into a fixed point in Poincaré map. As the rotational speed is increased to a certain value, the rotor system motion will no longer perform the synchronous motion as a result of nonlinear

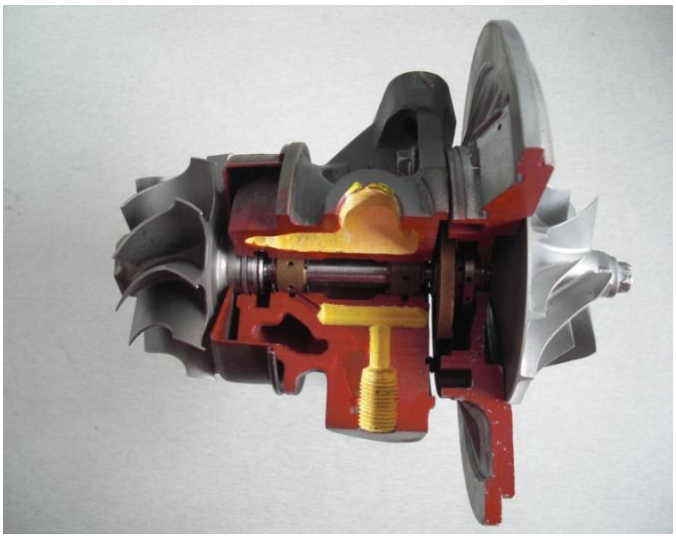

Figure 1. Turbocharger rotor system.

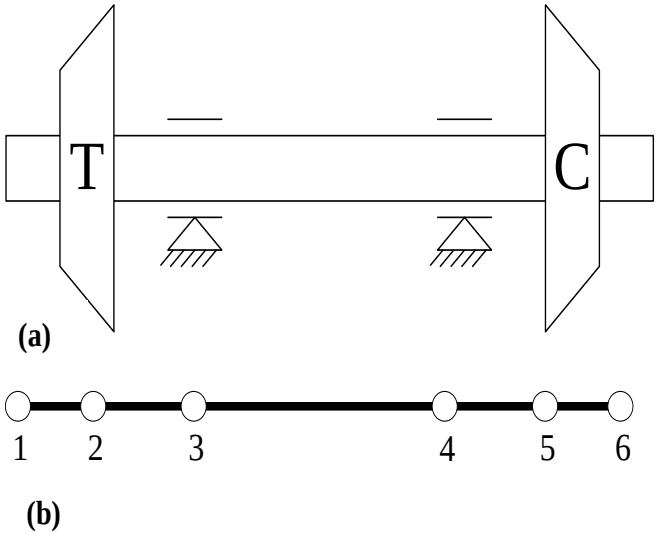

Figure 2. (a) Physical model of a turbocharger rotor system (b) Lumped model of a turbocharger rotor system.

hydrodynamic forces. A bifurcation occurs at that speed. According to the floquet theory, the bifurcation style can be deduced by from where and at which speed that the maximum floquet multiplier crosses the unit circle (Frulla, 2000). If the maximum floquet multiplier crosses the unit circle through (1.0), the periodic solution encounters a saddle-node bifurcation; if the maximum floquet multiplier crosses the unit circle through (-1.0), the periodic solution encounters a period-doubling bifurcation. After the bifurcation, the system performs a period k motion, which maps into k independent fixed points in Poincaré map; if the maximum floquet multiplier crosses the unit as the conjugate complex, the periodic solution encounters a hopf bifurcation. After the bifurcation, the system performs a quasi-period motion, which maps into a closed curve in Poincaré map. If a group of points are irregularly mapped in Poincaré map, it can be deduced that the system enters into the chaos.

MODELING FOR A TURBOCHARGER ROTOR SYSTEM

The lumped model for a turbocharger rotor system

As shown in Figure 1, a turbocharger rotor system consists of turbine and compressor impellers on a shared shaft supported by a pair of floating ring bearings. The physical and lumped model are shown in Figure 2(a) and (b). The turbocharger rotor is modeled as six mass nodes linked by elastic shaft segments.

As the mass and moment of inertia of the rotor are assumed to be distributed on the node, the system mass matrix will become diagonalised, which is shown in Equation (13).

$$[M]=\mathrm{diag}(M_1, M_1)$$
$$[M_1]=\mathrm{diag}(m_1, Jd_1, m_2, Jd_2, \ldots, m_6, Jd_6) \quad (13)$$

The system rotation matrix is expressed by Equation (14).

$$[J]=\begin{bmatrix} 0 & J_1 \\ -J_1 & 0 \end{bmatrix}$$
$$[J_1]=\mathrm{diag}(0, Jp_1, 0, Jp_2, \ldots, 0, Jp_6) \quad (14)$$

The gyroscopic matrix is then derived in Equation (15).

$$[G]=\Omega[J] \quad (15)$$

The material of the turbocharger shaft is assumed to be uniformed and then stiffness matrix of the rotor system can be expressed as follows:

$$[K]=\mathrm{diag}(K_1, K_1)$$

$$[K_1]=\begin{bmatrix} [K_{11}]_1 & [K_{12}]_1 & & & & & \\ [K_{21}]_1 & [K_{22}]_1+[K_{11}]_2 & [K_{12}]_2 & & & & \\ & [K_{21}]_2 & [K_{22}]_2+[K_{11}]_3 & [K_{12}]_3 & & & \\ & & [K_{21}]_3 & [K_{22}]_3+[K_{11}]_4 & [K_{12}]_4 & & \\ & & & [K_{21}]_4 & [K_{22}]_4+[K_{11}]_5 & [K_{12}]_5 & \\ & & & & [K_{21}]_5 & [K_{22}]_5 & \end{bmatrix}$$

$$[K_{11}]_i=\frac{EI}{l_i}\begin{bmatrix} 12 & 6l_i \\ 6l_i & 4l_i^2 \end{bmatrix}, [K_{22}]_i=\frac{EI}{l_i}\begin{bmatrix} 12 & -6l_i \\ -6l_i & 4l_i^2 \end{bmatrix},$$
$$[K_{12}]_i=[K_{21}]_i=\frac{EI}{l_i}\begin{bmatrix} -12 & 6l_i \\ -6l_i & 2l_i^2 \end{bmatrix} \quad (16)$$

As far as the turbocharger rotor system is concerned, the primary exciting forces for the bending vibration include the static and dynamic loads. Static loads denote the lubricant feed pressure exerted on the ring, the dead weight, etc. Dynamic loads denote the forces with varied values, such as the rotor imbalance, the

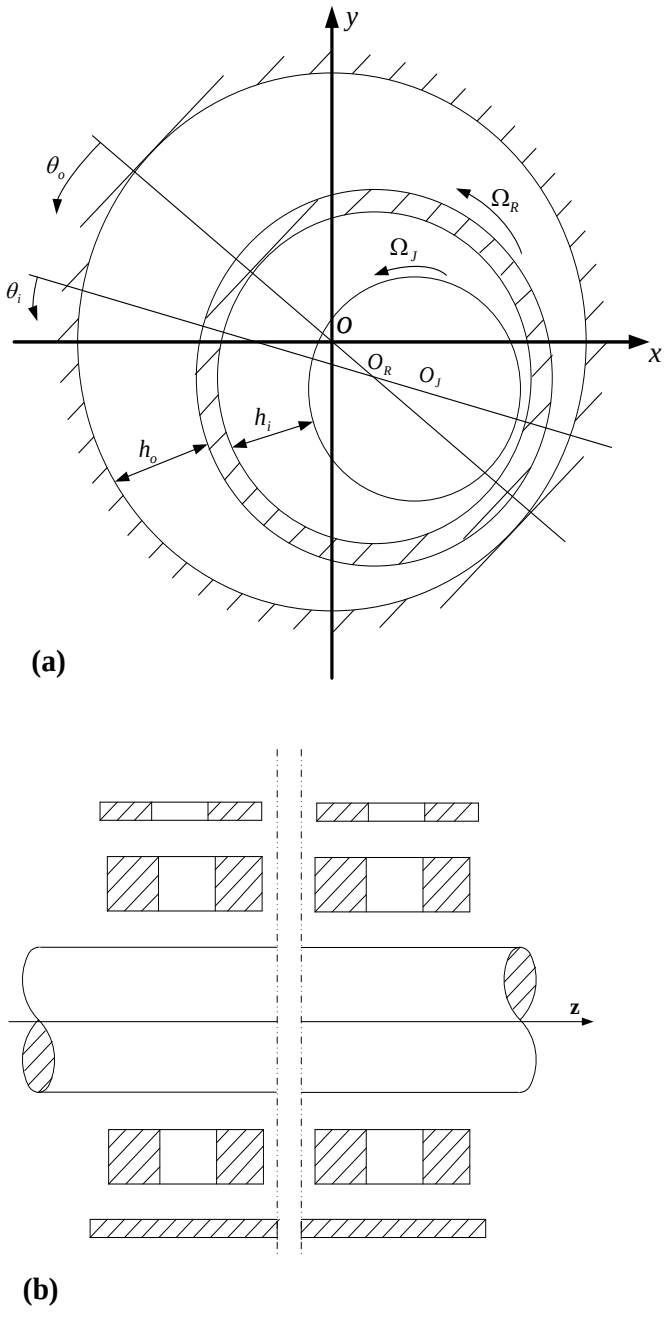

Figure 3. Coordinate system of the floating ring bearing.

hydrodynamic fluid force, etc.

The motion equation for the turbocharger rotor system is expressed as:

$$[M]\{\ddot{U}\}+[C+G]\{\dot{U}\}+[K]\{U\}=-\{W\}+\{F_u\}+\{Fh_{inner}\} \quad (17)$$

where

$$\{U\}=\{x_1, \theta_{y1}, x_2, \theta_{y2}, ..., x_6, \theta_{y6}, y_1, \theta_{x1}, y_2, \theta_{x2}, ..., y_6, \theta_{x6}\}$$

represent displacement vectors in the horizontal and vertical directions, that is, the X and Y directions. On the right hand side of the equation, the primary exciting forces include the imbalance centrifugal force $\{F_u\}$, the hydrodynamic force of the inner oil film $\{Fh_{inner}\}$ and the dead weight $\{W\}$.

The motion of the ring is determined by hydrodynamic forces in outer and inner oil films, the dead weight of the ring and the lubricant feed pressure. Therefore, the motion equation for the ring is given by:

$$[M_R]\{\ddot{U}_R\}=\{Fh_{outer}\}-\{Fh_{inner}\}-\{W_R\}-\{P\} \quad (18)$$

where $\{U_R\}$ represents the displacement vector of the ring, and $[M_R]$ is the mass matrix of the ring. The exciting force vectors include hydrodynamic forces of the two oil films, the lubricant feed pressure and the dead weight.

The motion equation for the turbocharger rotor system is then expressed in Equation (19).

$$\begin{bmatrix}[M] & [0]\\ [0] & [M_R]\end{bmatrix}\begin{Bmatrix}\ddot{U}\\ \ddot{U}_R\end{Bmatrix}+\begin{bmatrix}[C+G] & [0]\\ [0] & [0]\end{bmatrix}\begin{Bmatrix}\dot{U}\\ \dot{U}_R\end{Bmatrix}+\begin{bmatrix}[K] & [0]\\ [0] & [0]\end{bmatrix}\begin{Bmatrix}U\\ U_R\end{Bmatrix}=\{F\}$$

$$\{F\}=\begin{Bmatrix}F_u\\ 0\end{Bmatrix}-\begin{Bmatrix}W\\ W_R\end{Bmatrix}-\begin{Bmatrix}0\\ P\end{Bmatrix}+\begin{Bmatrix}Fh_{inner}\\ Fh_{outer}-Fh_{inner}\end{Bmatrix} \quad (19)$$

In order to improve the accuracy of the numerical integration, the motion equation of the turbocharger rotor system is normalized, which is expressed by Equation (20).

$$[\overline{M}]\{\ddot{\overline{U}}\}+[\overline{C}+\overline{G}]\{\dot{\overline{U}}\}+[\overline{K}]\{\overline{U}\}=\{\overline{F}\} \quad (20)$$

The dimensionless parameters are listed as follows:

$$\overline{U}=U/(Ci+Co),\ \overline{\Omega}=\Omega\sqrt{(Ci+Co)/g},\ \tau=\Omega_J t,$$

$$[\overline{M}]=\begin{bmatrix}[M] & [0]\\ [0] & [M_R]\end{bmatrix}(Ci+Co)\overline{\Omega}_J^2,$$

$$[\overline{C}+\overline{G}]=\begin{bmatrix}[C+G] & [0]\\ [0] & [0]\end{bmatrix}(Ci+Co)\overline{\Omega}_J,$$

$$[\overline{K}]=\begin{bmatrix}[K] & [0]\\ [0] & [0]\end{bmatrix}(Ci+Co),\ \overline{F}=F(\tau,\overline{U})$$

Nonlinear hydrodynamic forces

Figure 3 shows the coordinate system of the floating ring bearing, hydrodynamic forces can be derived from the oil film pressure distribution. In this paper, Capone oil film force model has been extended to the floating ring bearing. The analytical expressions of hydrodynamic forces in the outer and inner oil films are expressed as follows (Capone et al., 1991):

Table 1. Simulation parameters.

Simulation parameter	Value
Mass of the turbine node (kg)	1.4
Diameter moment of inertia of the turbine node (kgm^{-2})	6.3×10^{-4}
Polar moment of inertia of the turbine node (kgm^{-2})	1.26×10^{-5}
Mass of the compressor node (kg)	1.0
Diameter moment of inertia of the compressor node (kgm^{-2})	4.5×10^{-4}
Polar moment of inertia of the compressor node (kgm^{-2})	9×10^{-4}
Mass of the ring (kg)	0.02
Outer radius of the ring (m)	9×10^{-3}
Inner radius of the ring (m)	6×10^{-3}
Outer bearing clearance (m)	8×10^{-5}
Inner bearing clearance (m)	2×10^{-5}
Lubricant viscosity in the inner film (Pas)	0.006
Lubricant viscosity in the outer film (Pas)	0.012
Length of the bearing (m)	0.01
Young's modulus (GPa)	205
Length of the turbocharger rotor (m)	0.15

$$\begin{Bmatrix} Fh_{outer\_x} \\ Fh_{outer\_y} \end{Bmatrix} = -\mu_o \Omega_R \left(\frac{R_o^2}{C_o^2}\right)\left(\frac{L^2}{D_o^2}\right)(R_o L)\frac{\sqrt{(x_R - 2\dot{y}_R)+(y_R + 2\dot{x}_R)}}{(1 - x_R\cos\theta - y_R\sin\theta)} \begin{Bmatrix} 3x_R V_o - \sin\alpha_o G_o - 2\cos\alpha_o S_o \\ 3y_R V_o - \cos\alpha_o G_o - 2\sin\alpha_o S_o \end{Bmatrix}$$

$$V_o = \frac{2 + (y_R\cos\alpha_o - x_R\sin\alpha_o)G_o}{(1 - x_R^2 - y_R^2)}$$

$$G_o = \frac{\pi}{\sqrt{1 - x_R^2 - y_R^2}} - \frac{2}{\sqrt{1 - x_R^2 - y_R^2}}\tan^{-1}\left(\frac{y_R\cos\alpha_o - x_R\sin\alpha_o}{\sqrt{1 - x_R^2 - y_R^2}}\right)$$

$$S_o = \frac{(x_R\cos\alpha_o + y_R\sin\alpha_o)}{(1 - x_R^2 - y_R^2)}$$

$$\alpha_o = \tan^{-1}\left(\frac{y_R + 2\dot{x}_R}{x_R - \dot{y}_R}\right) - \frac{\pi}{2}\text{sign}\left(\frac{y_R + 2\dot{x}_R}{x_R - \dot{y}_R}\right) - \frac{\pi}{2}\text{sign}(y_R + 2\dot{x}_R) \quad (21)$$

$$\begin{Bmatrix} Fh_{inner\_x} \\ Fh_{inner\_y} \end{Bmatrix} = -\mu_i \left(\Omega_J + \frac{R_i}{R_J}\right)\left(\frac{R_J^2}{C_i^2}\right)\left(\frac{L^2}{D_i^2}\right)(R_J L)\frac{\sqrt{(x_i - 2\dot{y}_i)+(y_i + 2\dot{x}_i)}}{(1 - x_i\cos\theta - y_i\sin\theta)} \begin{Bmatrix} 3x_i V_i - \sin\alpha_i G_i - 2\cos\alpha_i S_i \\ 3y_i V_i - \cos\alpha_i G_i - 2\sin\alpha_i S_i \end{Bmatrix}$$

$$V_i = \frac{2 + (y_i\cos\alpha_i - x_i\sin\alpha_i)G_i}{(1 - x_i^2 - y_i^2)}$$

$$G_i = \frac{\pi}{\sqrt{1 - x_i^2 - y_i^2}} - \frac{2}{\sqrt{1 - x_i^2 - y_i^2}}\tan^{-1}\left(\frac{y_i\cos\alpha_i - x_i\sin\alpha_i}{\sqrt{1 - x_i^2 - y_i^2}}\right)$$

$$S_i = \frac{(x_i\cos\alpha_i + y_i\sin\alpha_i)}{(1 - x_i^2 - y_i^2)}$$

$$\alpha_i = \tan^{-1}\left(\frac{y_i + 2\dot{x}_i}{x_i - \dot{y}_i}\right) - \frac{\pi}{2}\text{sign}\left(\frac{y_i + 2\dot{x}_i}{x_i - \dot{y}_i}\right) - \frac{\pi}{2}\text{sign}(y_i + 2\dot{x}_i) \quad (22)$$

SIMULATION RESULTS AND ANALYSIS

Based on the developed model, bending vibration of the turbocharger rotor system has been simulated in MATLAB. According to simulation results, the effects of the rotor imbalance and lubricant feed pressure on the stability of the rotor system are studied. It should be noted that due to the material and mass distribution, the bending vibration on the compressor side is generally more dramatically compared to that on the turbine side. Therefore, researches focus on the motion of the shaft on the compressor side. The dimensionless speed range considered in this paper is from 1 to 10. Table 1 lists the simulation parameters in the study of the stability of the turbocharger rotor system.

Rotational speed of the ring

When the shaft of the turbocharger spins, the ring will rotate in the same direction as the shaft due to the shear-

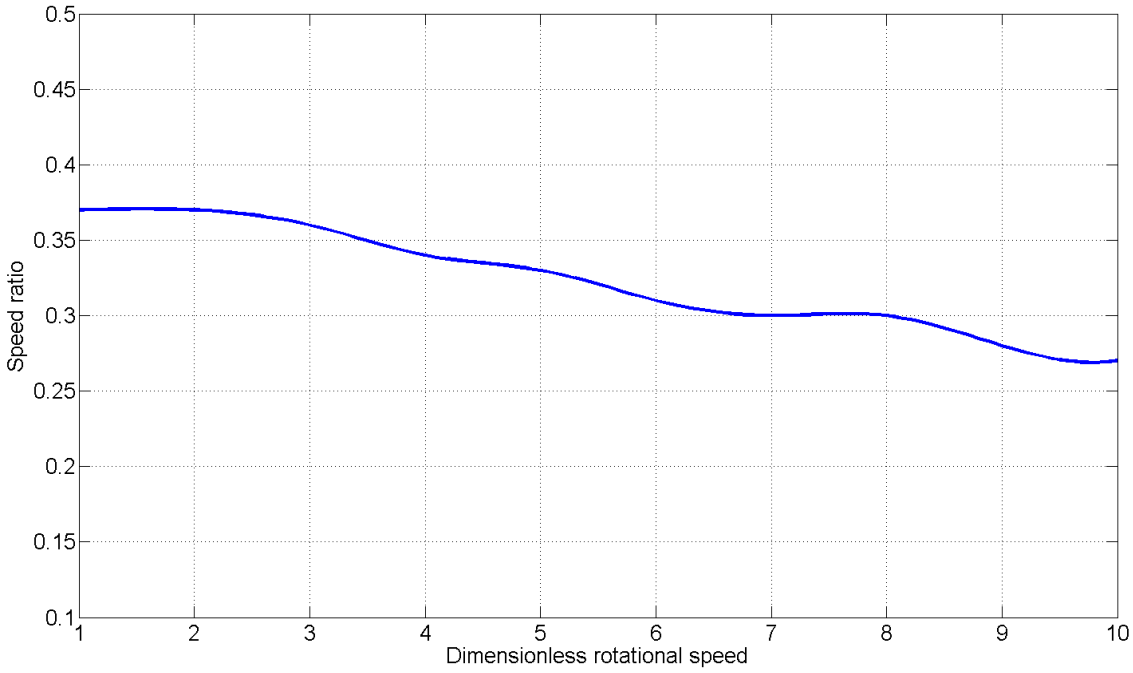

Figure 4. The speed ratio between ring and journal.

driven torques of inner and outer oil films. In the conventional lubrication theory, the speed ratio between ring and journal is viewed as a constant, which depends on geometrical parameters and the lubricant viscosity. However, experimental results and the recent theoretical research reveal that thermal effects on the performance of floating ring bearings cannot be ignored. The speed ratio between ring and journal is related to the shaft speed rather than a constant.

In order to obtain accurate results, the model developed by San (2004) is adopted in this paper. The relationship between ring speed and shaft speed is calculated, which is shown in Figure 4. The calculation result is then substituted into the dynamics model.

Influence of the rotor imbalance

Although the turbocharger has generally been balanced before being used, it is impossible to completely eliminate the rotor imbalance. The centrifugal force caused by the residual rotor imbalance can affect the rotor system motion and the stability. Here, it is initially assumed that the same eccentricities exerted on both turbine and compressor impellers, whilst the phase difference between them is zero. It should be noted that the centrifugal force generated on the turbine is larger than that on the compressor under the same values of the eccentricity because of a greater mass on the turbine impeller.

Under 0.1 eccentricities on both turbine and compressor nodes, as shown in Figures 5(a) and 5(b), the inner oil film instability occurs within the speed range of 4 to 5, when the rotor performs a period 2 motion. At the speed of 9, the outer oil film instability is excited. The rotor system motion undergoes the period 4 and the quasi-period motion. Under 0.2 eccentricities on both turbine and compressor nodes, as shown in Figures 5(c) and 5(d), a period-doubling bifurcation is encountered at the speed of 3 and the rotor performs a period 2 motion until the speed of 6, when the rotor system resumes stable. The outer oil film instability occurs at the speed of 6.3, during which the rotor performs a quasi-period motion. Under 0.3 eccentricities on both turbine and compressor nodes, as shown in Figures 5(e) and 5(f), the rotor system motion is dominated by the synchronous motion until the speed of 4, when the instability is excited in the inner oil film. As the speed is further increased, the period-doubling bifurcation occurs repeatedly and the system enters into chaos at the speed of around 5 and then the inner oil film instability disappears and the synchronous component dominates the system motion again. At the speed of 8.4 and over, the outer oil film instability occurs.

Figure 6 show the orbit, Poincaré map and the spectrum of the bending vibration of the journal at the speed of 5 under 0.1, 0.2 and 0.3 eccentricities respectively on both turbine and compressor nodes. At the speed of 5, the subsynchronous component of 0.5 of the shaft speed appears under 0.1, 0.2 and 0.3 eccentricities representing the inner oil film instability is excited. Under 0.1 and 0.2 eccentricities, the rotor

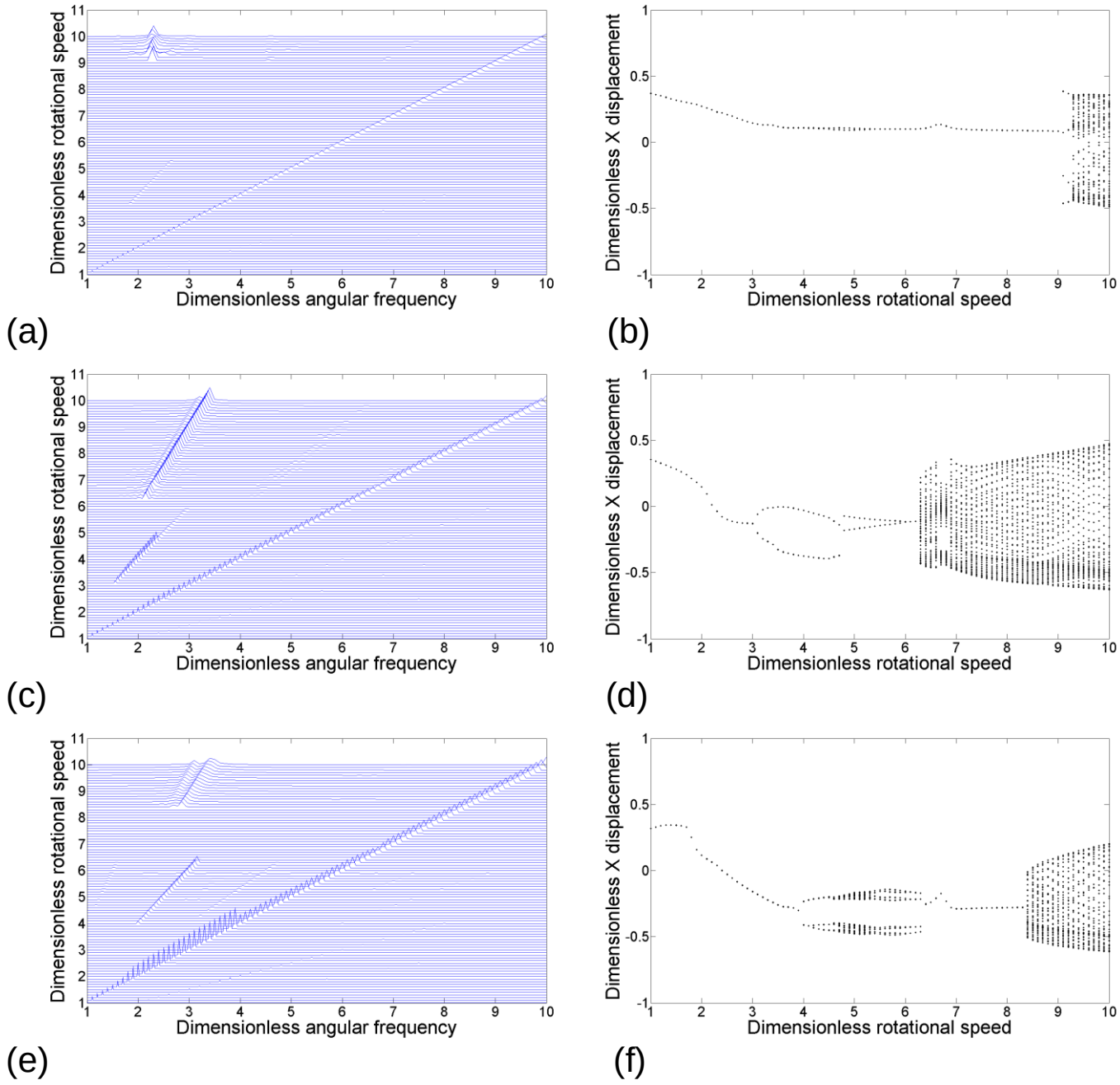

Figure 5. Waterfall and bifurcation diagrams of bending vibration of the journal on the compressor side under 0.1, 0.2 and 0.3 eccentricities on turbine and compressor nodes.

performs the period 2 motion, whilst under 0.3 eccentricity the rotor system motion enters into chaos via successive period-doubling bifurcations. The amplitude of the bending vibration becomes larger as the eccentricity is increased.

Figure 7 show the orbit, Poincaré map and the spectrum of bending vibration of the journal at the speed of 9 under 0.1, 0.2 and 0.3 eccentricities respectively on both turbine and compressor nodes. Under 0.1 eccentricity, the synchronous component dominates the rotor system motion at the speed of 9. The subsynchronous component of around 0.3 of the shaft speed is excited under 0.2 and 0.3 eccentricities indicating the appearance of the outer oil film instability. The rotor performs a quasi-period motion during the outer oil film instability.

Figure 8 shows the starting and ending speeds of the instabilities in the inner and outer oil films under different

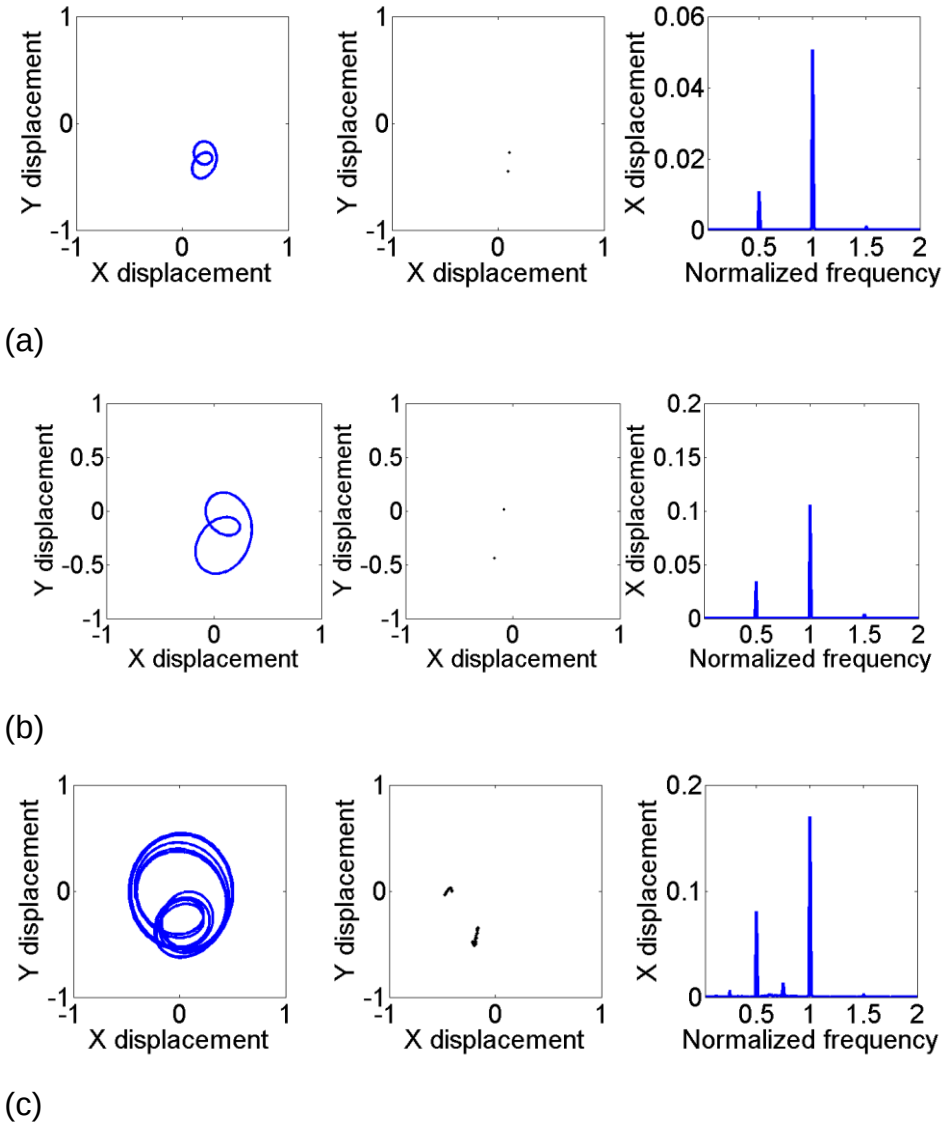

Figure 6. Bending vibration of the journal on the compressor side at $\overline{\Omega} = 5$: (a) under 0.1 eccentricity (b) under 0.2 eccentricity (c) under 0.3 eccentricity.

eccentricity on both turbine and compressor nodes. As the eccentricities are increased on both turbine and compressor nodes, the starting speed of the inner oil film instability initially drops and then raises. The inner oil film instability occurs at the lowest speed under 0.22 eccentricity on turbine and compressor nodes. The ending speed of the inner oil film instability gradually increases. On the other hand, the outer oil film instability occurs at a high speed under a small eccentricity. As the eccentricity is increased to 0.14, the threshold speed of the outer oil film instability dramatically drops and then gradually rises as the rotor imbalance is further increased.

To study the influences of rotor imbalance on the turbine impeller, bending vibration of the turbocharger rotor system under different eccentricities on the turbine node have been calculated, while the eccentricity on the compressor node is assumed to 0.3. The waterfall and bifurcation diagrams of the rotor system motion are displayed in Figure 9.

Under 0.1 eccentricity on the turbine node, as shown in Figures 9(a) and 9(b), the rotor runs stable below the speed of 3.1. Within the speed range of 3.1 to 5.6, the instability occurs in the inner oil film and the rotor performs a period 2 motion, that is, a synchronous component and a subsynchronous component of 0.5 of the shaft speed. At the speed of 8.9, a hopf bifurcation is encountered indicating the outer oil film instability. Under 0.2 eccentricity on the turbine node, as shown in Figures 9(c) and 9(d), the inner oil film instability occurs between

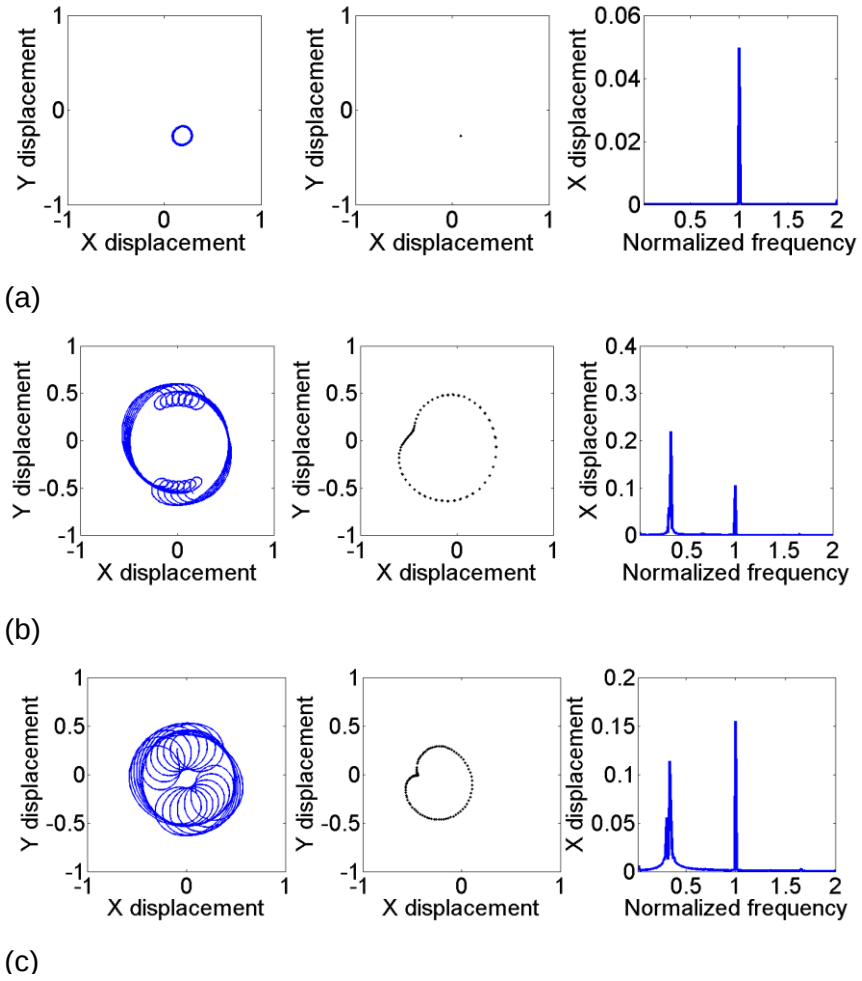

Figure 7. Bending vibration of the journal on the compressor side at $\overline{\Omega} = 9$: (a) under 0.1 eccentricity (b) under 0.2 eccentricity (c) under 0.3 eccentricity.

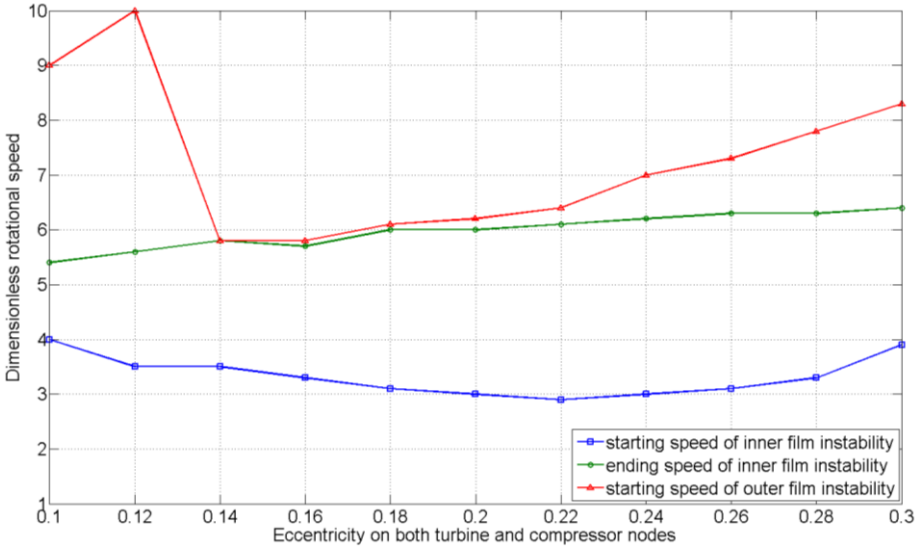

Figure 8. The starting and ending speeds of the instabilities in the inner and outer oil films under different eccentricity on both turbine and compressor nodes.

the speed of 3 and 6, during which the period-doubling bifurcation occurs twice. The rotor system motion undergoes the period 2, period 4 and period 2 motion successively. When the speed is increased to 8.3, the instability is excited in the outer oil film and the rotor performs a quasi-period motion. Under 0.3 eccentricity on the turbine node, as shown in Figures 9(e) and 9(f), the period-doubling bifurcation occurs continuously during the inner oil film instability and the rotor system motion enters into chaos at the speed of around 5.

Figure 10 shows the starting and ending speeds of the instabilities in the inner and outer oil films under different eccentricity on the turbine node. As the rotor imbalance is increased on the turbine node, both the starting and ending speeds are enhanced. When the eccentricity is greater than 0.28, the starting speed of the inner oil film instability raises sharply, which lead to a decrease of the duration of the inner oil film instability. The starting speeds of the outer oil film instability locate around the speed of 8.3, but increased obviously when the eccentricity is greater than 0.32.

In order to investigate the influence of rotor imbalance on the compressor impeller, bending vibration of the turbocharger rotor system under different eccentricities on the compressor node have been calculated. The waterfall and bifurcation diagrams of the rotor system motion are displayed in Figure 11.

Under 0.1 eccentricity on the compressor node, as shown in Figures 11(a) and 11(b), the inner oil film instability occurs within the speed range of 3 to 6.4. The rotor runs the period 2 and period 4 motion. At the speed of 8.3, the outer oil film instability is excited. A period-doubling bifurcation and a hopf bifurcation occur successively as the rotational speed is increased. The similar situations can be seen between the vibration under 0.2 and 0.3 eccentricities on the compressor node, which are shown in Figures 11(c), 11(d) and 11(e), 11(f) respectively. During the inner oil film instability, the rotor system motion enters into chaos status via multiple period-doubling bifurcations. When the instability is excited in the outer oil film, the rotor performs the quasi-period motion.

Figure 12 shows the starting and ending speeds of the instabilities in the inner and outer oil films under different eccentricity on the compressor node. The larger the eccentricity on the compressor node, at a higher speed the instability occurs in the inner oil film. The change of the ending speed of the inner oil film instability is not obvious. Therefore, the speed range of the inner oil film instability decreases under a larger eccentricity on the compressor node. As the eccentricity is increased on the compressor node, the threshold speed of the outer oil film instability becomes lower initially and then rises when the eccentricity exceeds 0.25.

The above analysis is on the basis of the rotor imbalance placing in the same direction. However, the phase difference cannot be ignored between the rotor imbalance on both turbine and compressor impellers. In this section, the effect of phase difference on the stability of the turbocharger rotor system is discussed. The value of eccentricity is assumed to 0.2 on two impellers.

Figure 13 show the waterfall and bifurcation diagrams of the journal vibration under 0°, 40°, 90°, 130°, 180° phase difference between the rotor imbalance which are 0.2 eccentricities on both impellers. When the rotor imbalance is in the same direction, as shown in Figure 13(a) and 13(b), the rotor performs a period 2 motion during the inner oil film instability between the speed range of 3 and 6. The outer oil film instability occurs at the speed of 6.3, when a hopf bifurcation is encounted. When the phase difference is 40°, as shown in Figure 13(c) and 13(d), the rotor performs a period 3 motion since the speed of 8 and then shows a quasi-period motion as the speed is further increased. When the phase difference is greater than 90°, both the inner and outer oil film instabilities become weaker, especially for the rotor imbalance placing in an opposite direction, when the instability is not excited in the inner oil film.

Influence of lubricant feed pressure

In the turbocharger, the lubricant is supplied into the outer clearance of the floating ring bearing through the oil path. The effect of the lubricant feed pressure on the dynamics performance of the turbocharger rotor system is studied by adjusting the static load on the ring. The value of the static load is the product of the lubricant feed pressure and the area of the supply hole, which is 0.5 cm^2 in this paper. Figure 14 show the waterfall and bifurcation diagrams of bending vibration of the journal on the compressor side under 0.3 eccentricities on both impellers under 10^5Pa (14(a), 14(b)), 1.5×10^5Pa (14(c), 14(d)) and 2×10^5Pa (14(e), 14(f)).

It can be seen that the higher the lubricant feed pressure provided, the more times period-doubling bifurcation encountered during the inner oil film instability. The amplitude of the rotor system also becomes larger within the speed range of the inner oil film instability.

Figure 15 illustrates the starting and ending speeds of the instabilities in the inner and outer oil films under different lubricant feed pressure. For the inner oil film, the ending speed of the instability raises as a higher lubricant feed pressure is supplied, whilst the change of the starting speed is not obvious. Therefore, the speed range of the inner oil film instability has been extended as increasing the lubricant feed pressure. For the outer oil film, the threshold speed of the instability is gradually increased as raising the supply pressure.

Conclusion

In this paper, a lumped model is developed for a

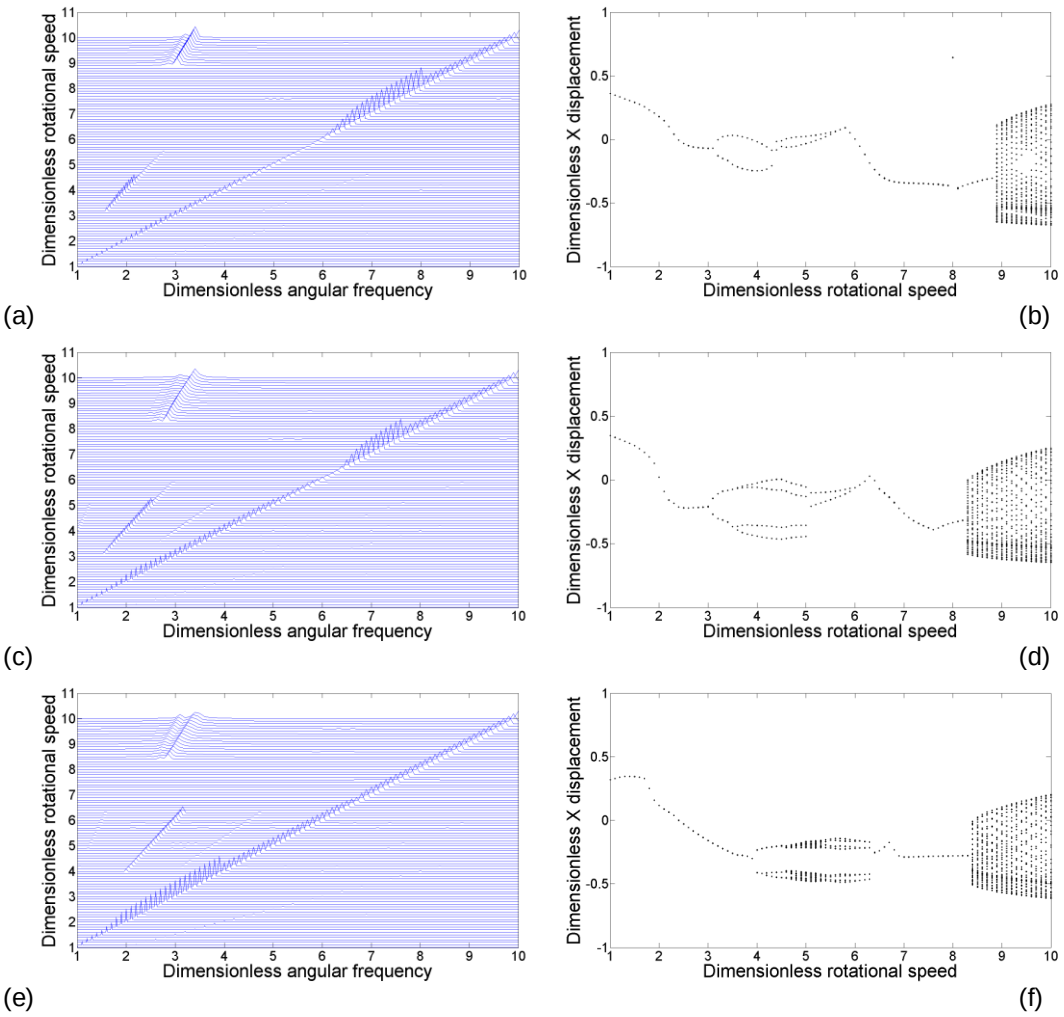

Figure 9. Waterfall and bifurcation diagrams of bending vibration of the journal on the compressor side under 0.1, 0.2 and 0.3 eccentricities on the turbine node and 0.3 eccentricity on the compressor node.

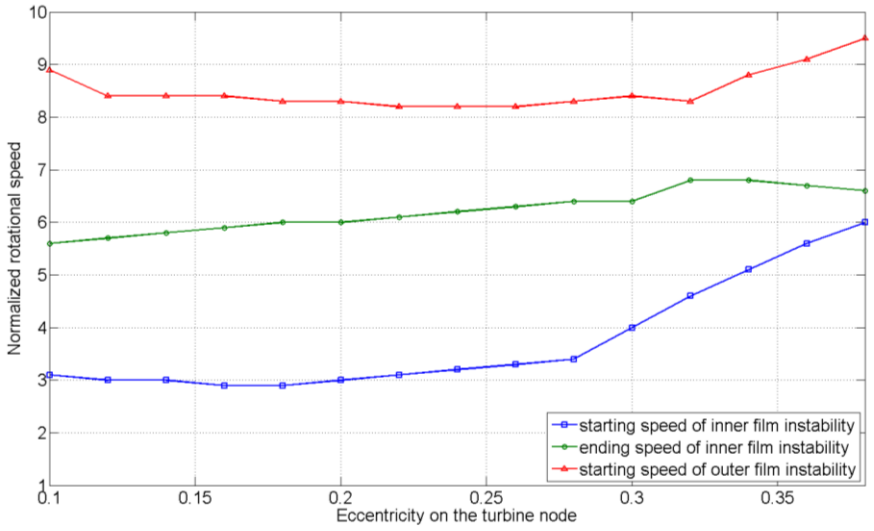

Figure 10. The starting and ending speeds of the instabilities in the inner and outer oil films under different eccentricity on the turbine node.

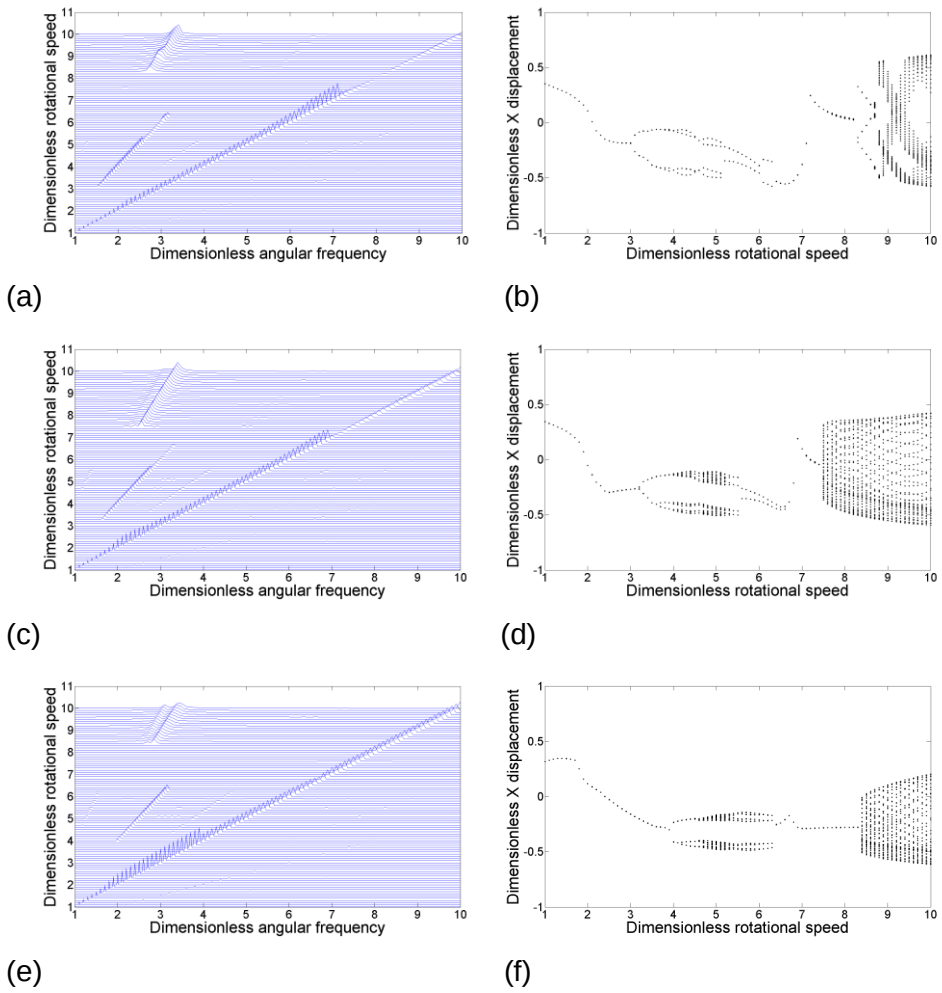

Figure 11. Waterfall and bifurcation diagrams of bending vibration of the journal on the compressor side under 0.1, 0.2 and 0.3 eccentricities on the compressor node and 0.3 eccentricity on the turbine node.

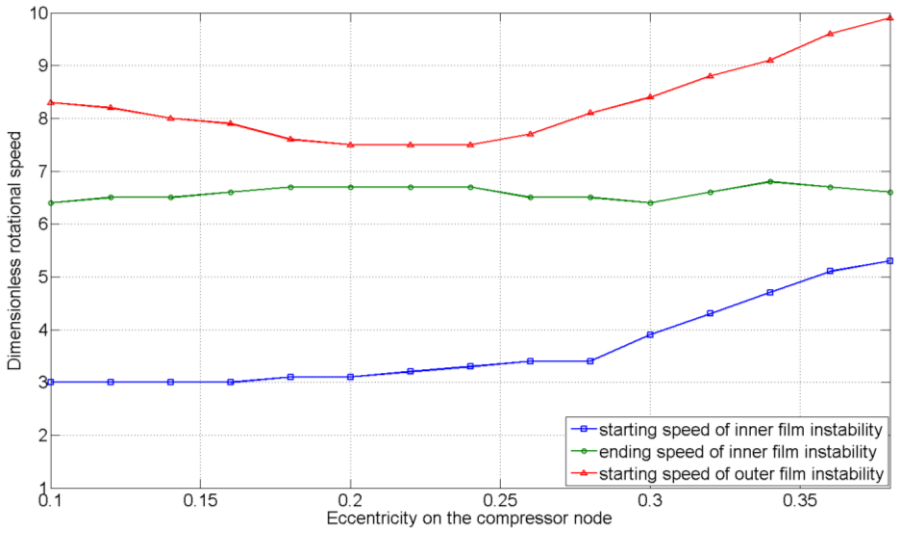

Figure 12. The starting and ending speeds of the instabilities in the inner and outer oil films under different eccentricity on the compressor node.

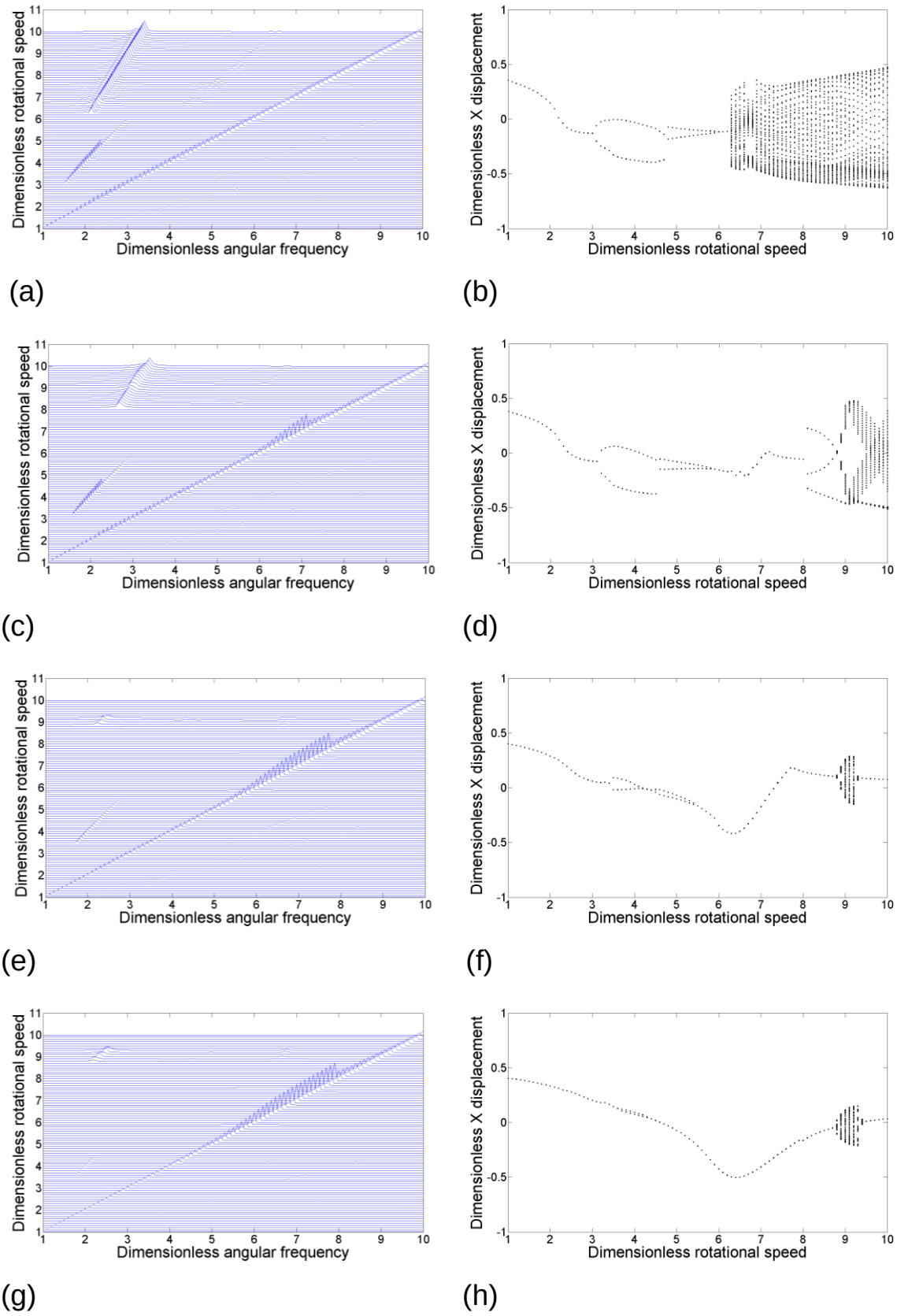

Figure 13. Waterfall and bifurcation diagrams of bending vibration of the journal on the compressor side under 0°, 40°, 90°, 130°, 180° phase difference respectively between the rotor imbalance of two impellers.

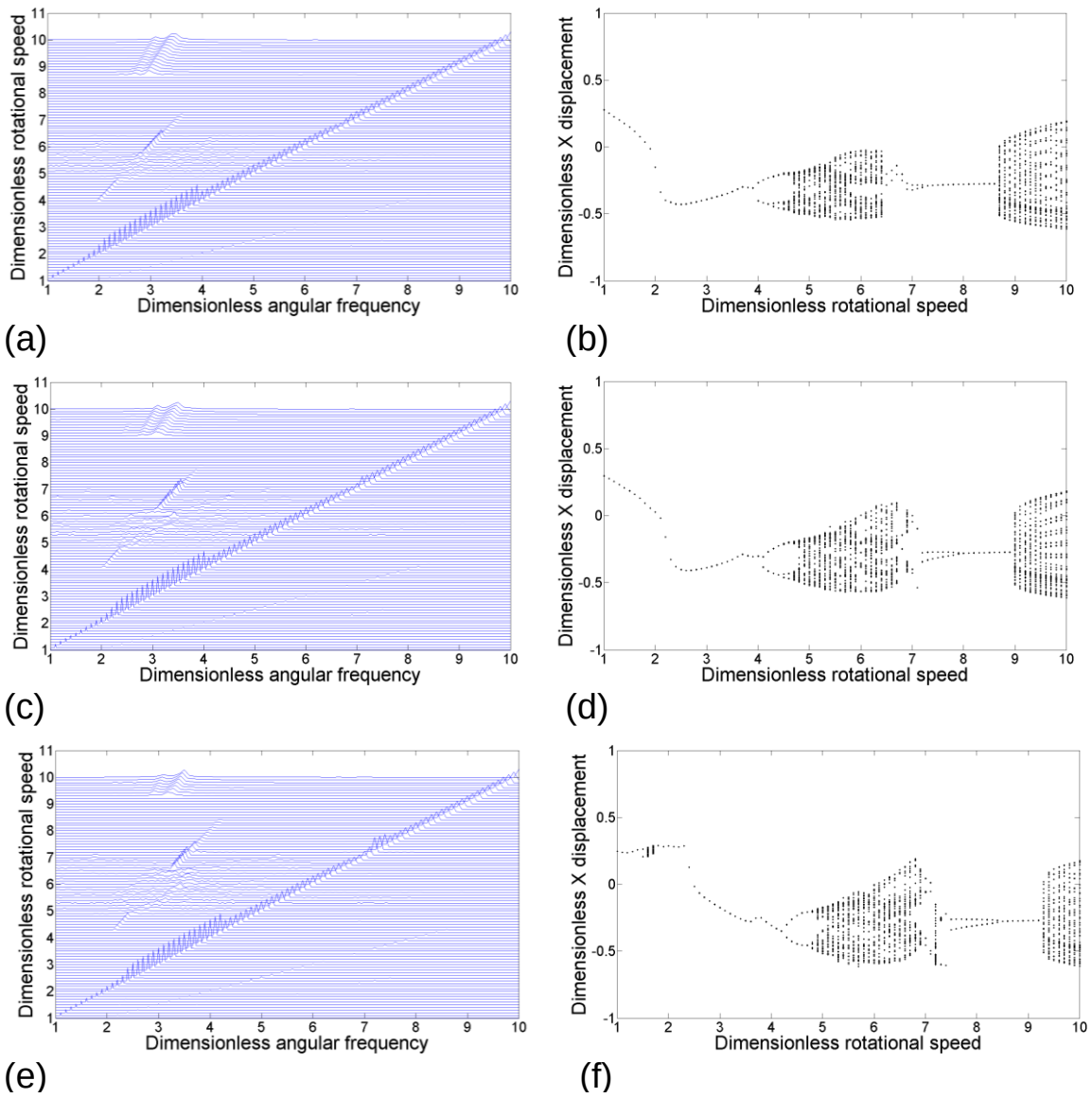

Figure 14. Waterfall and bifurcation diagrams of bending vibration of the journal on the compressor side under 10^5Pa, 1.5×10^5Pa and 2×10^5Pa lubricant feed pressure.

turbocharger rotor system supported by a pair of floating ring bearings considering the gyroscopic effect. The exciting forces include rotor imbalance, hydrodynamic force, lubricant feed pressure and the dead weight. The analytical expression of nonlinear hydrodynamic force in the inner and outer oil films is derived based on the Capone oil film force model. Following model development, bending vibration of the rotor system is simulated by MATLAB.

The shooting method and continuation algorithm are used to calculate the periodic solution of the turbocharger rotor system within the dimensionless speed range of 1 to 10. The stability of the rotor system motion and bifurcation style are analyzed by the floquet theory and Poincaré map.

Based on the calculation results, the effects of the rotor imbalance and lubricant feed pressure on the stability of the turbocharger rotor system are studied. The rotor of turbocharger generally performs a period k motion during the inner oil film instability and a quasi-period motion during the outer oil film instability. Under a small rotor imbalance, the starting speeds of both inner and outer oil film instabilities become lower as increasing the rotor imbalance, whilst under a large rotor imbalance, the imbalance centrifugal force can inhibit the appearance of the oil film instability. Moreover, a larger rotor imbalance can increase the number of times of the period-doubling bifurcation during the inner oil film instability.

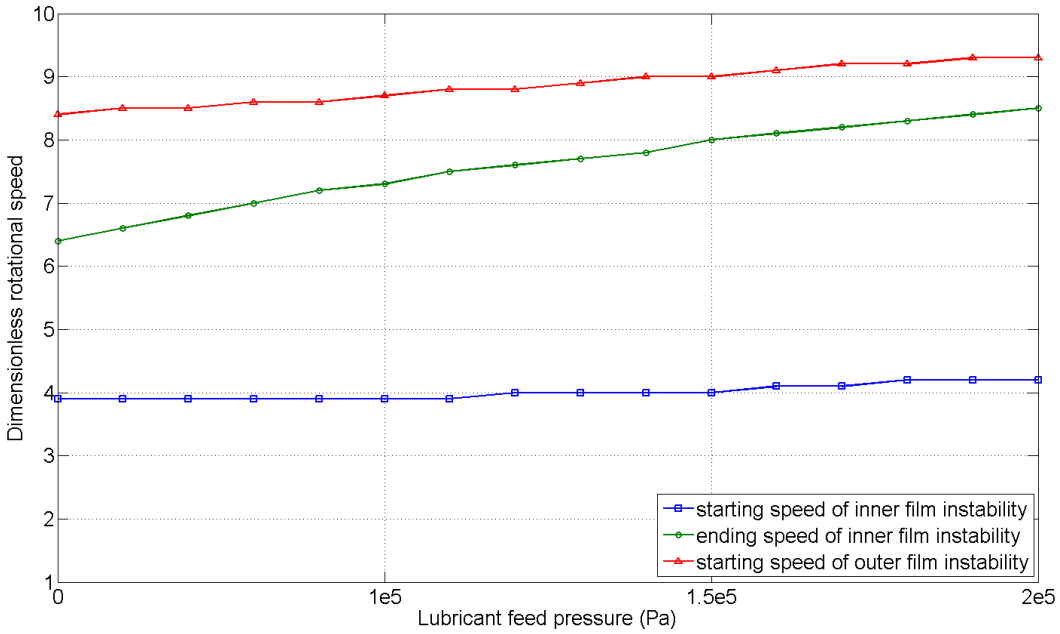

Figure 15. The starting and ending speeds of the instabilities in the inner and outer oil films.

The phase difference between the rotor imbalance on two impellers affect significantly the stability of the rotor system motion. When the phase difference is larger than 90^o, instabilities are obviously inhibited in both inner and outer oil films.

Increasing the lubricant feed pressure can extend the speed range of the inner oil film instability, during which the system enters into chaos via multiple period-doubling bifurcation.

Nomenclature: $[M]$, Mass matrix; $[M_R]$, Mass matrix of the ring; $[C]$, Damping matrix; $[K]$, Stiffness matrix; $[J]$, Rotation matrix; $[G]$, Gyroscopic matrix; $\{U\}$, Displacement vector; $\{U_R\}$, Displacement of the ring; $\{F\}$, Force vector; $\{F_u\}$, Imbalance centrifugal force; $\{Fh_{inner}\}$, Hydrodynamic force of inner oil film; $\{Fh_{outer}\}$, Hydrodynamic force of outer oil film; $\{P\}$, Lubricant feed pressure; $\{W\}$, Dead weight; $\{W_R\}$, Dead weight of the ring; $m_{1...6}$, Mass of nodes (kg); $Jd_{1...6}$, Diameter moment of inertia of nodes (kgm^2); $Jp_{1...6}$, Polar moment of inertia of nodes (kgm^2); $l_{1...5}$, Length of shaft segments (m); Ω, Rotational speed (rad/s); Ω_J, Journal speed (rad/s); Ω_R, Ring speed (rad/s); I, Unit matrix; P(u), Poincaré map; G(u), Residual function; μ_o, Lubricant viscosity of outer oil film (PaS); μ_i, Lubricant viscosity of inner oil film (PaS); C_o, Outer bearing clearance (m); C_i, Inner bearing clearance (m); R_o, Outer radius of the ring (m); R_i, Inner radius of the ring (m); R_J, Radius of the journal (m); L, Length of the bearing (m); D_o, Outer diameter of the ring (m); D_i, Inner diameter of the ring (m); x_R, Displacement of the ring in x direction (m), y_R, Displacement of the ring in y direction (m), $\dot{x}_R$, Velocity of the ring in x direction (m/s); $\dot{y}_R$, Velocity of the ring in y direction (m/s); x_i, Relative displacement of the journal in x direction (m); y_i, Relative displacement of the journal in y direction (m); $\dot{x}_i$, Relative velocity of the journal in x direction (m/s); $\dot{y}_i$, Relative velocity of the journal in y direction (m/s); EI, Bending stiffness (Nm^2).

REFERENCES

Aretakis N, Mathioudakis K, Kefalakis M, Papailiou K (2004). Turbocharger unstable operation diagnosis using vibroacoustics measurements. J. Eng. Gas Turbine Power 126(4):840-847.

Capone G (1991). Descrizione analitical del campo di forze fluidodinamico nei cuscinetti cilindrici lubrificati. L'Energia Elettrica. 68(3):105-110.

Chang-Jian CW, Chen CK (2006a). Bifurcation and chaos of a flexible rotor supported by turbulent journal bearings with non-linear suspension. P. I. Mech. Eng. J-J. Eng. 220(6):549-561.

Chang-Jian CW, Chen CK (2006b). Nonlinear dynamic analysis of a flexible rotor supported by micropolar fluid film journal bearings. Int. J. Eng. Sci. 44(16):1050-1070.

Chang-Jian CW, Chen CK (2007a). Chaos and bifurcation of a flexible rub-impact rotor supported by oil film bearings with non-linear suspension. Mech. Mach. Theory 42(3):312-333.
Chang-Jian CW, Chen CK (2007b). Bifurcation and chaos analysis of a flexible rotor supported by turbulent long journal bearings. Chaos Sol. Fractals 34(4):1160-1179.
Chen H, Hakeem I, Martinez-Botas RF (1996). Modelling of a turbocharger turbine under pulsating inlet conditions. P. I. Mech. Eng. A-J. Power 210(5):397-408.
Chu F, Zhang Z (1998). Bifurcation and chaos in rub-impact jeffcott rotor system. J. Sound. Vib. 210(1):1-18.
Dworski J (1964). High-speed rotor suspension formed by full floating hydrodynamic radial and thrust bearings. J. Eng. Power-T. ASME 86:149-160.
Frulla G (2000). Rigid rotor dynamic stability using floquet theory. Eur. J. Mech. A-Solid. 19(1):139-150.
Fu YM, Zheng YF, Zhu SJ (2003). Analysis of the chaotic motion for a rotor system with a transverse crack. Acta. Mech. Solida. Sin. 16(1):74-80.
Glienicke J (1966). Experimental investigation of the stiffness and damping coefficients of turbine bearings and their application to instability prediction. Proc. Inst. Mech. Eng. 181(28):116-129.
Goldman P, Muszynska A (1994). Chaotic behavior of rotor/stator systems with rubs. J. Eng. Gas. Turb. Power-T ASME 116(3):692-701.
Granas A, Guenther RB, Lee JW (2012). Continuation and shooting methods for boundary value problems of Bernstein type. J. Fix. Point. Theory A 6(1):27-61.
Hagg AC (1956). Some dynamic properties of oil-film journal bearing with reference to the unbalance vibration of rotors. Appl. Mech. 23(2):302-305.
Hill HC (1950). Sliper bearings and vibration control in small gas turbine. T. ASME 80:1756-1764.
Howard SA (1999). Rotordynamics and design methods of an oil-free turbocharger. Tribol. T. 42(1):174-179.
Kreuz-Ihli T, Filsinger D, Schulz A, Wittig S (2000). Numerical and experimental study of unsteady flow field and vibration in radial inflow turbines. J. Turbomach. 122(2):247-254.
Lund JW (1964). Spring and damping coefficients for the tilting pad journal bearing. T. ASLE 7(4):342-352.
Lund JW (1968). Calculation of stiffness and damping properties of gas bearing. J. Lubric. Tech-T. ASME 90:793-803.
Payri F, Benajes J, Reyes M (1996). Modelling of a supercharger turbines in internal-combustion diesel engines. Int. J. Mech. Sci. 38(8):853-869.
Payri F, Desantes JM, Broatch A (2000). Modified impulse method for the measurement of the frequency response of acoustic filters to weakly nonlinear transient excitations. J. Acoust. Soc. Am. 107(2):731-738.
Peat KS, Torregrosa AJ, Broatch A, Fernández T (2006). An investigation into the passive acoustic effect of the turbine in an automotive turbocharger. J. Sound. Vib. 295(1):60-75.
Rohde SM, Ezzat HA (1980). Analysis of dynamically loaded floating ring bearings for automotive applications. J. Lubric. Tech-T. ASME 102:271-277.
Sternlicht B (1959). Elastic and damping properties of cylindrical journal bearings. J. Basic. Eng-T. ASME 81:101-108.
Tanaka M, Hori Y (1972). Stability characteristics of floating bush bearings. J. Lubric. Tech-T. ASME 93(3):248-259.
Tatara A (1970). An experimental study on the stability effect of floating bush journal bearings. B. JSME 13:859-863.
Trippett R, Dennis FC (1983). High-speed floating-ring bearing test and analysis. T. ASLE 27(1):73-81.
Yang JF, Liu ZS, Yu DR (2004). Research on nonlinear oil film force and its stability of journal bearing. Power Eng. 24(4):501-504.